Aerosol Science and Technology
Publication details, including instructions for authors and subscription information:
http://www.informaworld.com/smpp/title~content=t713656376

Determination of Particle Effective Density in Urban Environments with a Differential Mobility Analyzer and Aerosol Particle Mass Analyzer

Michael Geller [a]; Subhasis Biswas [a]; Constantinos Sioutas [a]
[a] Department of Civil & Environmental Engineering, University of Southern California, Los Angeles, California, USA

First Published on: 01 August 2006

To cite this Article: Geller, Michael, Biswas, Subhasis and Sioutas, Constantinos (2006) 'Determination of Particle Effective Density in Urban Environments with a Differential Mobility Analyzer and Aerosol Particle Mass Analyzer', Aerosol Science and Technology, 40:9, 709 — 723

To link to this article: DOI: 10.1080/02786820600803925
URL: http://dx.doi.org/10.1080/02786820600803925

Aerosol Science and Technology, 40:709–723, 2006

ISSN: 0278-6826 print / 1521-7388 online
DOI: 10.1080/02786820600803925

Determination of Particle Effective Density in Urban Environments with a Differential Mobility Analyzer and Aerosol Particle Mass Analyzer

Michael Geller, Subhasis Biswas, and Constantinos Sioutas
Department of Civil & Environmental Engineering, University of Southern California, Los Angeles, California, USA

Effective densities of atmospheric aerosols in various locations of the Los Angeles Basin were determined by a DMA-APM technique. Effective density was calculated by comparing voltage distributions of sampled atmospheric aerosols with PSL particles of known density. The five sites chosen for field experiments were: (1) Interstate-710 Freeway, impacted by heavy-duty diesel vehicles; (2) State Route CA-110, open only to gasoline vehicles; (3) Riverside, a receptor site known for secondary particle formation; (4) University of Southern California, a typical urban and industrial environment; and (5) Coast for marine aerosol. The size range selected for this study was from 50 nm to 414 nm. While 50 nm particles exhibited a single effective density multiple effective densities were measured for each of the other particle sizes as significant fractions of these particles are transported from background sources. Regardless of location, 322–414 nm particle effective densities were considerably lower than unity. The lowest effective densities ($\sim$0.1 g cm^{-3}) were reported for I-710, confirming that diesel combustion aerosols are rich in chain agglomerates with large void spaces. Riverside exhibited high effective densities ($\sim$1.2–1.5 g cm^{-3}) for 50–202 nm particles, which we hypothesize is due to transformations that occur during advection from Los Angeles. Measurements of diurnal variation of effective density at Riverside support this hypothesis. Overall, our results suggest that effective density declines as the particle mobility diameter increases irrespective of location. Fractal dimensions calculated from average effective densities were lowest for I-710 ($D_f = 2.41$) and CA-110 ($D_f = 2.54$) aerosols, presumably due to the influence of vehicular combustion emission on these sites. By contrast, average fractal dimensions at USC, Riverside and Coast were found to be 2.79, 2.83, and 2.92, respectively. High fractal dimensions at these sites may be the effects of aging, moisture absorption and/or organic vapor condensation on the particles, which fills void space and makes particles more spherical.

Received 13 December 2005; accepted 5 March 2006.

The authors would like to thank Tyler Beck from Particle Instruments, LLC. and Kanomax USA, Inc. for the use of the APM for this study. This research was supported by the Southern California Particle Center and Supersite (SCPCS), funded by EPA under the STAR program through Grant Nos. 53-4507-0482 and 53-4507-7721 to the University of Southern California. The research described herein has not been subjected to the agency's required peer and policy review and therefore does not necessarily reflect the views of the agency, and no official endorsement should be inferred. Mention of trade names or commercial products does not constitute an endorsement or recommendation for use.

Address correspondence to Constantinos Sioutas, University of Southern California, Department of Civil and Environmental Engineering, 3620 S. Vermont Avenue, Los Angeles, CA 90089, USA. E-mail: sioutas@usc.edu

INTRODUCTION

Recent toxicological and epidemiological research has found various adverse health effects related to fine and ultrafine particles (Dockery and Pope 1994; Peters et al. 1997; Li et al. 2003; Oberdörster et al. 1996). However, the mechanisms by which these health effects are elicited have not been determined, creating speculation that chemistry, surface area, number of particles, or a combination of these properties may be responsible. Additionally, a current review of epidemiological studies has found a relationship between freeways and cancer rates (Mack 2004). Ambient particles, unlike other gaseous co-pollutants, are unique in that their complete characterization would require knowledge of their size distribution, mass, and number concentrations as well as their chemical composition. All of these important parameters determine the site of particle deposition in the respiratory track and the degree to which they may exert adverse health effects.

In addition to the above list, particle density is an important parameter, because it determines the transport and depositional properties of particles in lungs. In most cases, the "average" particle density of a given size range (which, in most studies, is restricted to fine PM, or $PM_{2.5}$) is determined indirectly by knowing the bulk chemical composition of that range. Typically, this involves measurement of the relative mass fractions of key PM constituents, such as elemental and organic carbon (EC-OC), inorganic ions (sulfate, nitrate, and ammonium) and selected trace elements and metals. Atmospheric aerosol particles are often assumed to be completely spherical in shape, but combustion-generated particles are ubiquitously found to grow from nearly spherical primary particles into fractal-like

agglomerate structures with high carbon content. Combustion is a well-known source of fine and ultrafine particles and a source to which humans are frequently exposed, especially in relation to traffic and mobile sources. Diesel engines in particular emit large amounts of these agglomerate soot particles (Park et al. 2004; Burtscher 2005).

Agglomerate particles are characterized by high surface area and low density, both of which have implications in toxicity and deposition in the lungs. To account for particle morphologies substantially different from spherical shapes, the term "effective density" has often been employed in the aerosol field. Effective density is the ratio of mass to volume based on the mobility equivalent diameter and is defined by the following equation:

$$\rho_e = \frac{d_{ve}^3}{d_{me}^3}\rho_{\text{true}}, \quad [1]$$

where ρ_e is the effective density, d_{ve} is the volume equivalent diameter, d_{me} is the mobility equivalent diameter, and ρ_{true} is the bulk density of the material (McMurry et al. 2002).

The fractal dimension (D_f) is an indirect measure of the morphology of irregularly shaped agglomerate particles. Traditionally, light-scattering measurements as well as transmission electron microscopy (TEM) have been used to provide data on the soot fractal dimension. However, these methods are very tedious, as they only measure few particles at a time, and they cannot be used "on-line" to provide this information near-continuously. These methods also contribute to the discrepancy of soot aggregate properties; light-scattering data are heavily weighted by particles at the large end of the size distribution. TEM derivations of the fractal dimension of 3D objects are limited to a two-dimensional field, and thus suffer from problems of primary particle overlap, screening effects, and cluster anisotropy (Wentzel et al. 2003). The various measurement techniques presume different definitions for particle size, including radius of gyration, maximum length and mobility diameter. Kutz and Schmidt-Ott (1990) coupled a differential mobility analyzer (DMA) with an impactor to collect particles for TEM analysis. Although this study incorporated mobility diameter measurements, it still suffered from the TEM limitations discussed above.

Fractal dimension (D_f) can readily be measured if one knows the effective density of particles of difference sizes. The relationship is given by Park et al. (2003):

$$\rho_e = C d_{me}^{Df-3}, \quad [2]$$

where D_f is fractal dimension and C is a constant.

Researchers have used different experimental approaches to determine particle effective density. Few studies have been carried out to determine its seasonal and diurnal characteristics for $PM_{2.5}$ (Morawska et al. 1999; Kuhlbusch et al. 2001; Pitz et al. 2003). Hanel and Thudium (1977) determined the bulk dry aerosol density by measuring the volume and mass of particles, independently. As part of the Pittsburgh Supersite efforts, Khlystov et al. (2004) developed and algorithm to merge SMPS and APS distributions and combined them with MOUDI mass concentrations to determine aerosol density for size fractionated PM_{10}. Recently, researchers have employed a tandem set-up of a DMA and electrical low-pressure impactor (ELPI) for diesel particles (Maricq et al. 2000; Ahlvik et al. 1998). Virtanen et al. (2004) calculated effective density by simultaneously measuring the mobility and aerodynamic size distributions with an SMPS and an ELPI, using a best-fit technique to match distributions. These studies eliminate the need to visually inspect particles in order to estimate their fractal dimension, which increases the number of particles that can be sampled. Recent studies, however, have indicated rapid overloading in ELPI impactor stages due to the "fluffy" structure of diesel particles, reducing their usefulness (Van Gulijk et al. 2001). McMurry et al. (2002) developed a novel and elegant technique to measure particle effective density via a tandem differential mobility analyzer (TDMA) and aerosol particle mass analyzer (APM). The number of particles that can be sampled greatly increases with this method.

The present study employs the same DMA-APM set-up used by McMurry et al. (2002) to determine the effective density of various types of atmospheric aerosols in the Los Angeles Basin. Building upon the findings of the McMurry et al. (2002) study, which was conducted in one location and was restricted to two aerosol mobility diameters, our study's goal was to create a broader database of effective aerosol densities for different particle sizes in the range of 50 to 414 nm and at different locations in Southern California, each of which is impacted by distinct particle sources and formation mechanisms.

METHODS

Experimental Design

This study is based on a methodology similar to one developed by McMurry et al. (2002), in which a differential mobility analyzer (DMA) precedes the APM. A schematic of the DMA-APM setup is shown in Figure 1. A near-monodisperse aerosol of a known particle mobility diameter is selected by the DMA of the Scanning Mobility Particle Sizer (SMPS Model 3081, TSI Inc., St. Paul, MN), which is connected upstream of the APM (Model 10, Kanomax USA inc, Andover, NJ). The DMA is equipped with a Kr^{85} neutralizer that brings the aerosols to the Boltzmann equilibrium. The inlet and sheath flow rates in the DMA were 0.5 liters per minute (LPM) and 5.0 LPM, respectively. This configuration enables the system to select particles between 15 nm and 500 nm, affording flexibility to select both ultrafine and accumulation mode particles.

Ehara et al. (1996) first proposed the APM to classify particles according to their mass to charge ratios. Classification occurs between the narrow annular space, also termed the operating space, available between two rotating coaxial cylindrical electrodes. The outer cylinder (inner radius = 63 mm) is grounded while classifying voltage is applied to the inner cylinder (outer radius = 60 mm). The angular velocity of inner and outer

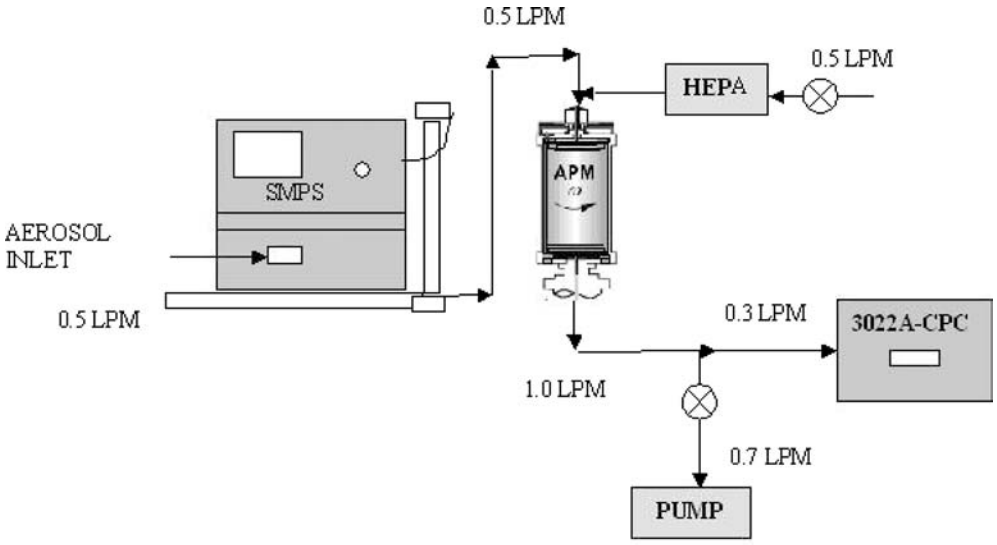

FIG. 1. Schematic diagram of DMA-APM set-up.

electrodes is the same. Therefore, when the aerosol is introduced into the operating space, it acquires the same angular velocity as that of the electrodes. Particles thus experience radial electrical and centrifugal forces, which act in opposite directions. When the forces balance each other, the particles will penetrate through the rotating cylinders to the downstream detector. The principal equation describing the force balance is:

$$m\omega^2 r = \frac{\pi d_{ve}^3}{6}\rho_{\text{true}}\omega^2 r = neE_{\text{APM}}, \quad [3]$$

where m is particle mass, ω is APM angular velocity, r is the radial distance to the annular gap from the axis of rotation, and E_{APM} is the electric field.

After selection by the DMA, particles mix with 0.5 LPM of particle-free air (HEPA capsule, Gelman laboratory) and then pass through the APM. A Condensation Particle Counter (CPC Model 3022A, TSI Inc., St. Paul, MN) counts those particles that have the APM-selected mass. The CPC operated at 0.3 LPM, therefore a diaphragm pump pulled an additional 0.7 LPM in order to satisfy the 1.0 LPM minimum flow requirement of the APM. Three APM rotational velocities (1000 RPM, 2000 RPM, 3000 RPM) were chosen in order to adequately measure the desired size range of particles. Higher rotational velocities make it possible to sample less massive particles. For each particle size, the voltage on the APM was scanned manually, and the particle concentrations corresponding to each voltage were recorded. The residence time of the APM was considered when matching particle concentrations measured by the CPC with their corresponding voltage settings on the APM. Thus, APM voltage was fixed for a time period much longer than its residence time to account for transient particle penetration between voltage steps. In addition, concentrations at the beginning and end of measurements at each voltage step were discarded.

PSL particle sizes were selected keeping in mind the limitations of both the DMA and the APM. The APM voltage corresponding to the maximum number concentration for the selected PSL particle size was used as the reference voltage ($V_{\text{APM PSL}}$) in Equations (4–6).

$$\frac{m_{\text{test}}\omega^2 r}{m_{\text{PSL}}\omega^2 r} = \frac{\rho_{\text{true}}\frac{\pi d_{ve}^3}{6}}{\rho_{\text{PSL}}\frac{\pi d_{\text{PSL}}^3}{6}} = \frac{neE_{\text{APM-sample}}}{neE_{\text{APM-PSL}}} = \frac{V_{\text{APM-sample}}}{V_{\text{APM-PSL}}}, \quad [4]$$

where, V_{APM} is the APM voltage for sample and PSL aerosols, and ρ_{PSL} is the material density of PSL particles.

For spherical particles $d_{ve} = d_{\text{me}} = d_{\text{PSL}}$, therefore

$$\rho_{\text{true(sphere)}} = \rho_{\text{PSL}}\frac{V_{\text{APM-sample}}}{V_{\text{APM-PSL}}}, \quad [5]$$

and the effective density of irregularly shaped particles can be given by

$$\rho_e = \rho_{\text{PSL}}\frac{V_{\text{APM-sample}}}{V_{\text{APM–PSL}}}. \quad [6]$$

Laboratory Experiments

Before performing ambient sampling, PSL particles between 50–414 nm were measured by the DMA-APM tandem to construct each particle's reference voltage distribution. Monodisperse polystyrene latex (PSL, Polyscience Inc., Warrington, PA) particles were generated by atomizing their respective solutions with a constant output Nebulizer (HEART, VORTRAN Medical Technology, Inc., Sacramento, CA). Sufficient dilution of HEPA-filtered, particle free dry room air was supplied in a 2-liter glass container to remove moisture from the nebulized particles.

Particles were neutralized by a series of Po-210 neutralizers (NDR Inc., Grand Island, NY) before entering the DMA-APM tandem. The density of PSL particles is 1.054 g cm^{-3}, which has been used as the reference density for particle effective density calculations.

Atmospheric Experiments

To determine the effective density of atmospheric particles with different characteristics, sampling was conducted at five locations in the Los Angeles Basin, each of which is influenced by varied emission sources and formation mechanisms (Figure 2). The sampling period extended from early September to late October of 2005, with 5–7 days spent at each site. The University of Southern California's Particle Instrumentation Unit of the Southern California Supersite (USC) represents a typical urban/traffic/industrial environment. It is about 100 m downwind of CA-110 freeway and 2 miles south of downtown Los Angeles. The next sampling location was a site 5 meters away from I-710 freeway in Downey, CA. This eight-lane freeway is a major heavy commercial truck route with approximately 25–30% diesel truck traffic (Zhu et al. 2002). Previous studies have shown that a relatively high elemental carbon content and low effective density characterizes particles generated due to diesel combustion (Sharma et al. 2005; Burtscher 2005; Keskinen et al. 1998). State Route 110 (CA-110), between downtown Los Angeles and Pasadena, CA (USA) is the oldest freeway in the United States and thus cannot accommodate large trucks. It offers a unique opportunity to sample particles generated predominantly by light-duty gasoline vehicles. The sampling location is in the Hermon Park within 2–3 meters from the edge of the freeway. The Riverside site is situated within the facilities of the Citrus Research Center and the Agricultural Experiment Station of the University of California, Riverside. It is a receptor site, as aged particles from Los Angeles are advected to the site by the westerly winds (Geller et al. 2002). It is also influenced by the upwind stationary ammonia sources that react with advected NOx to form ammonium nitrate. In addition, Riverside is a typical location for photochemical organic aerosol formation due to high solar radiation that contributes to temperatures often in excess of 30°C during the afternoon. Coastal aerosols were measured at El Segundo beach on the Pacific coast. This site is impacted by marine aerosols comprised mainly of sea salt and organic compounds. The average number concentration in the afternoon is very low, typically in the range of 2,000–5,000 particles cm^{-3} (Biswas et al. 2005) because the onshore flow during the afternoon is stronger. The concentrations at this site may be slightly higher in the morning when the offshore flow from overnight moves the more polluted urban mix towards the coast, where it stagnates (Hughes et al. 1999). Finally, we measured effective densities of particles generated by a brush fire, which flared up during the study period. Sampling occurred on one afternoon at a location within two miles downwind of the fire. The opportunistic nature of this event and the relative unpredictability of the fire and wind directions allowed for measurement of only two particle sizes.

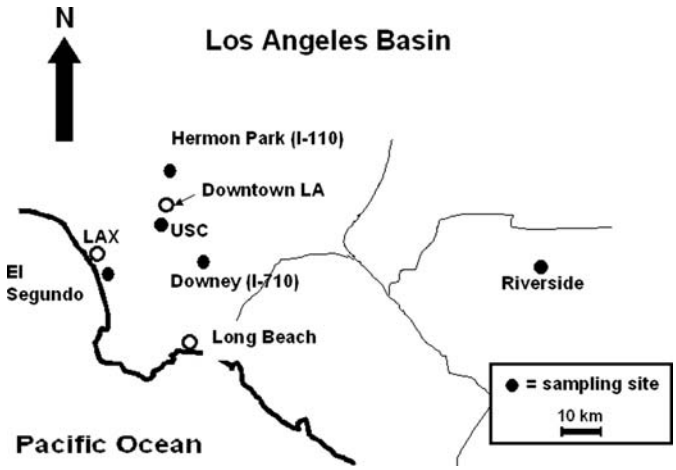

FIG. 2. Location of sampling sites.

RESULTS AND DISCUSSION

Laboratory Experiments

The first phase of the laboratory evaluation was to determine the reference APM voltages for particles of known size and density. Before scanning the voltage with the APM, the DMA was connected directly to the CPC to confirm the mode particle diameter of the PSL number concentration and the degree to which each aerosol was monodisperse. The DMA was set to the voltage (or mobility diameter) corresponding to the maximum number concentration from the mobility scan. An iterative process of varying voltage and rotational velocity allowed us to select a set of APM operating parameters to scan voltages within the range of the instrument. Table 1 summarizes the APM operating characteristics, and Figure 3 illustrates particle number concentrations (N) penetrating the APM as a function of APM voltage for all sampled PSL particle sizes. Due to the large variation between number concentrations of different particle sizes, N for 50 nm PSL is plotted on the primary (left) y-axis, while all other PSL sizes are plotted on the secondary (right) y-axis. It is evident from this figure that small changes in particle diameter equate to

TABLE 1
APM sampling parameters

Particle diameter (nm)	Rotational velocity (RPM)	PSL peak voltage (V)
50	3000	14
118	2000	75
146	2000	140
202	1000	130
322	1000	760
414	1000	1660

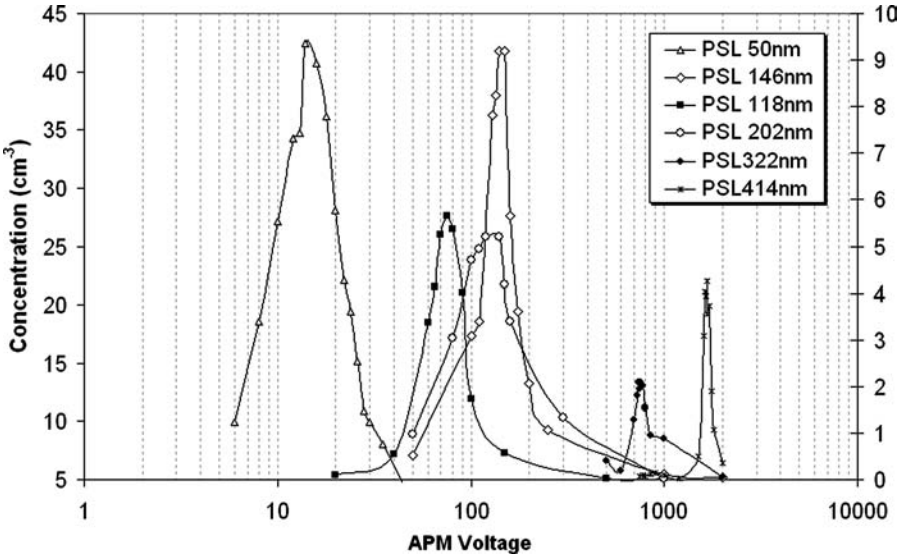

FIG. 3. Number concentration downstream of APM versus APM classifying voltage for PSL spheres.

large variations in APM voltage. Because of constraints of the APM, 50 nm particles were the smallest reliably sampled in this study, and the greater width of the voltage distribution at this size is most likely the result of proximity to the limit of detection (LOD) of the APM. The APM operating characteristics for each particle size remained constant throughout all successive experiments.

Spatial Variability of Density

The apparent particle density depends on many parameters, including temperature and humidity, radiation, wind conditions, and atmospheric mixing (Pitz et al. 2003). Thus, effective density is expected to be quite variable and uncorrelated to a single meteorological or particulate measurement parameter. Since this study focuses on the effective density variability based on size and site, care was taken to ensure that data were recorded during periods that are representative of the prevailing ambient conditions in the Los Angeles Basin. A case study presenting preliminary results on diurnal variation of effective density is presented later in this discussion, but further analysis is beyond the scope of this study.

Samples were usually taken during the afternoon hours (12:00–16:00) at each location in order to minimize the bias due to diurnal density changes. Because sampling at each site occurred during a defined short time interval, multiple scans for each particle size were similar. Approximately 2–4 scans lasting between 30–60 minutes each for every particle size were recorded, of which representative scans at each location are presented. In addition to sampling within the prescribed time interval, representative scans were selected such that the times of the scans nearly coincided at each location. Table 2 describes the local weather conditions at each site on the days sampled. With the exception of Riverside, temperatures and relative humidities are generally comparable between sites. Riverside's location about 100 km inland and in the vicinity of Southern California deserts accounts for its distinctive meteorology, which in general led to warmer and drier conditions compared to the rest of the sites.

Upon completion of the reference measurements, the system was deployed at all prescribed field locations. The following section discusses the associations between effective density and particle size at the different field locations. A figure showing a typical DMA-APM voltage scan is presented in Figure 4. The peaks of the voltage distribution were used to determine effective densities, and the data are summarized in Table 3. In some locations, data could not be collected for a particle size because ambient concentrations were below the detection limit of the instrument.

As previously mentioned, 50 nm was the lowest particle size selected for effective density measurements. Also noted earlier, 50 nm is near the LOD of the APM, which is likely to be a reason for broadening of the voltage distributions for these particles. The effective densities at I-710, CA-110, and USC are around unity, which, along with the assumption that these particles are close to spherical, is likely explained by condensation

TABLE 2
Ambient temperature and relative humidity ranges for all sampling locations

Sampling location	Temp (°C)	RH (%)
USC	20.0–22.2	55.0–63.0
Interstate-110 freeway	20.1–25.6	36.0–66.0
Riverside	23.3–31.7	11.0–56.0
Coast	16.7–21.1	71.0–93.0
Interstate-710 freeway	19.4–26.7	45.0–84.1

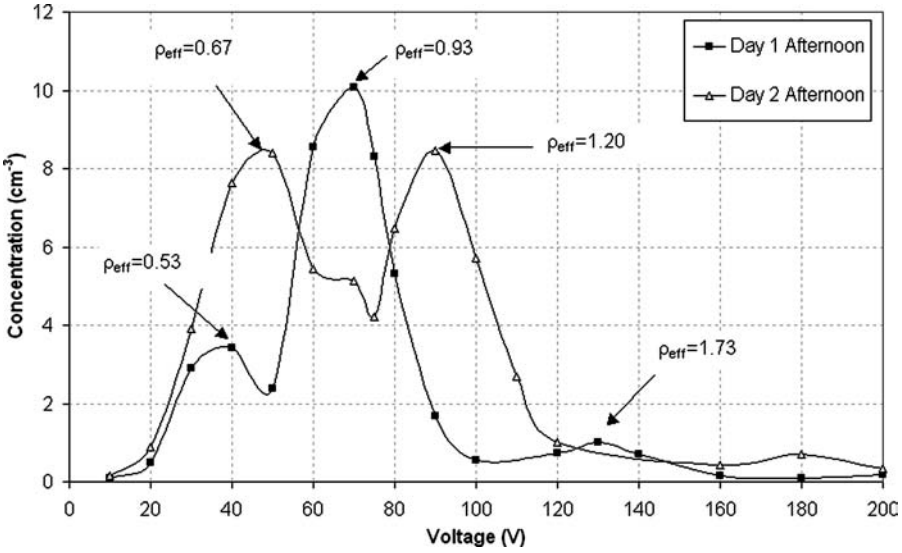

FIG. 4. Number concentration through DMA-APM as a function of APM voltage for atmospheric particles at I-710 with $d_{me} = 118$ nm.

of organic vapors onto a solid core particle. These three sites are most influenced by vehicular sources, which emit semivolatile particles, mostly found in the sub-50 nm range following nucleation and growth processes (Harris and Maricq 2001; Sakurai et al. 2003). Maricq et al. (2004) reported $\rho_e = 1.2$ g cm^{-3} for 50 nm diesel soot by using an Electrical Low Pressure Impactor (ELPI) and SMPS while Park et al. (2003) stated a density of $\sim$1 g cm^{-3} by comparing SMPS and filter mass measurements.

Previous studies at CA-110 have demonstrated that these particles may be internally or externally mixed, depending on size, and are highly volatile in nature (Kuhn et al. 2005 a,b). USC and CA-110 had two measured effective densities, 0.98 g cm^{-3}/1.51 g cm^{-3} and 1.24 ± 0.05 g cm^{-3}/1.65 g cm^{-3}, respectively, suggesting externally mixed aerosol populations. This range of densities may be explained by particles being a mixture of chemical components, the majority of which is composed of elemental carbon, organic carbon, and water vapor. Organic speciation of ultrafine particles from dynamometer and tunnel studies has yielded a component known as the unresolved complex mixture (UCM), which resembles motor oil ($\rho \sim 0.87$ g cm^{-3}) in gas chromatograph traces (Phuleria et al. 2006; Schauer et al. 1999). Black carbon has a density between 1.8 and 2.1 g cm^{-3} (Lide 1992), and organic compounds can have densities between 0.77 and 1.90 g cm^{-3} (Turpin and Lim 2001). Thus, a particle containing some amount of each will likely exhibit a density that is an average of its component densities.

Coastal 50 nm particles demonstrated an effective density of 0.90 g cm^{-3}. Interestingly, Turpin and Lim (2001) estimated nearly the same aerosol density for San Nicolas Island, a background site for Los Angeles. Coastal marine aerosols predominantly consist of organics with high moisture content, which may lead to such low effective density particles (Jaffe et al. 2005). It is also possible that particles emitted from ships anchored off the Southern California coast affect the coastal site at certain times, which would also justify the low measured density. It should be noted that USC and coastal measurements of 50 nm particles produced the widest voltage distributions, which may be due to low concentrations at these sites that may result in statistical uncertainty.

It is evident from Table 3 that the average measured effective density of 50 nm particles at Riverside, 1.41 ± 0.12 g cm^{-3}, differs significantly from the other locations. The number-based particle size distributions in that location during the photochemically active period (defined in Los Angeles as the period between April through October) are bimodal, with a distinct mode between 40–60 nm and another at 90–110 nm (Kim et al. 2002). The smaller mode particles, which are likely organic in nature, are thought to be generated by photochemical reactions (Blando and Turpin 2000; Jang et al. 2002), whereas the larger mode particles represent an aged aerosol advected eastward to that area of Riverside from central Los Angeles (Fine et al. 2004). Historically, the density of secondary organic aerosol (SOA) was estimated by elaborate chemical speciation and mathematical calculations (Bahreini et al. 2005). It is difficult, however, to identify the complete composition of SOA due to instrumental limitations that prevent us from identifying all species formed by these atmospheric reactions. An effective density of approximately 1.4 g cm^{-3} is expected for unseeded SOA aerosols as most of the organic precursors are of similar density (Bahareini et al. 2005).

All sites, with the exception of I-710 and CA-110, have 118 nm particles with effective densities greater than unity. CA-110 and I-710 emissions contained particles with effective densities as low as 0.70 g cm^{-3} and 0.56 g cm^{-3}, respectively, indicating the presence of chain agglomerates with fractal dimensions <3.0. The 710 freeway is influenced by heavy-duty

TABLE 3
Summary of APM measurements conducted in the Los Angeles Basin in September/October 2004

			APM Voltage, V			Number Concentration, cm^{-3}			Effective Density, g cm^{-3}			Aerodynamic diameter, nm		
Location	Date	Time	V_1	V_2	V_3	N_1	N_2	N_3	ρ_{e1}	ρ_{e2}	ρ_{e3}	d_{ae1}	d_{ae2}	d_{ae3}
$d_{me} = 50$ nm														
710	9/20/2005	16:45–18:00	13	—	—	10.5	—	—	0.98	—	—	50	—	—
	9/21/2005	14:15–15:00	16	—	—	10.0	—	—	1.20	—	—	53	—	—
110	9/26/2005	15:30–16:30	17	—	—	7.3	—	—	1.28	—	—	54	—	—
	9/28/2005	13:00–13:30	16	22	—	6.5	4.2	—	1.20	1.66	—	53	59	—
USC	9/8/2005	16:00–17:00	13	20	—	1.0	0.7	—	0.98	—	—	50	—	—
Coast	9/23/2005	16:15–17:00	12	—	—	1.0	—	—	0.90	—	—	48	—	—
Riverside	9/27/2005	14:45–15:15	17	—	—	2.5	—	—	1.28	—	—	54	—	—
	9/29/2005	14:30–15:00	20	—	—	2.8	—	—	1.51	—	—	57	—	—
	9/29/2005	16:00–16:30	19	—	—	3.0	—	—	1.43	—	—	56	—	—
$d_{me} = 118$ nm														
710	9/20/2005	8:30–10:00	40	60	—	15.0	19.9	—	0.56	0.84	—	97	111	—
	9/20/2005	13:00–14:00	40	70	—	3.4	10.1	—	0.56	0.98	—	97	117	—
	9/21/2005	8:45–9:45	—	80	160	—	20.8	3.7	—	1.12	2.25	—	123	155
	9/21/2005	13:15–14:15	50	90	—	8.4	8.5	—	0.70	1.26	—	105	128	—
110	9/26/2005	12:45–13:45	70	90	—	5.3	7.7	—	0.98	1.26	—	117	128	—
	9/26/2005	16:30–17:00	70	100	—	1.7	3.5	—	0.98	1.41	—	117	132	—
	9/28/2005	13:30–14:15	50	100	—	1.1	2.5	—	0.70	1.41	—	105	132	—
USC	9/8/2005	17:00–18:00	—	75	—	—	3.8	—	—	1.05	—	—	120	—
Coast	9/23/2005	12:15–13:15	—	90	165	—	1.4	0.4	—	1.26	2.32	—	128	156
Riverside	9/27/2005	10:30–11:15	—	100	175	—	2.0	0.3	—	1.41	2.46	—	132	159
	9/27/2005	12:30–13:15	—	100	190	—	2.3	0.2	—	1.41	2.67	—	132	164
	9/29/2005	12:30–13:00	—	105	—	—	1.1	—	—	1.48	—	—	134	—
	9/29/2005	15:30–16:00	—	100	—	—	1.5	—	—	1.41	—	—	132	—
Fire	9/30/2005	13:15–13:45	—	100	—	—	11	—	—	1.41	—	—	132	—
$d_{me} = 202$ nm														
710	9/20/2005	10:00–11:15	50	—	180	8.8	—	0.6	0.41	—	1.46	149	—	229
	9/20/2005	14:30–15:15	50	100	220	10.8	6.9	0.5	0.41	0.81	1.78	149	188	245
	9/21/2005	9:45–10:15	—	115	250	—	12.5	0.9	—	0.93	2.03	—	197	256
	9/21/2005	11:45–12:45	—	130	—	—	6.3	—	—	1.05	—	—	206	—
110	9/26/2005	13:45–14:30	40	130	—	1.3	3.2	—	0.32	1.05	—	139	206	—
	9/26/2005	17:00–17:30	40	140	—	1.3	1.3	—	0.32	1.14	—	139	211	—
	9/28/2005	14:15–15:00	40	140	200	1.3	1.5	0.5	0.32	1.14	1.62	139	211	237
USC	9/12/2005	11:00–12:00	—	150	290	—	2.9	0.4	—	1.22	2.35	—	216	269
	9/13/2005	15:00–16:00	—	130	—	—	1.4	—	—	1.05	—	—	206	—
	9/14/2005	11:00–12:00	40	130	300	0.9	1.8	0.5	0.32	1.05	2.43	139	206	272
	9/14/2005	13:00–13:45	—	130	260	—	1.3	0.4	—	1.05	2.11	—	206	259
Coast	9/23/2005	13:15–14:15	—	120	260		1.7	0.5		0.97	2.11	—	200	259
Riverside	9/27/2005	9:00–10:00	60	130	—	1.9	3.8	—	0.49	1.05	—	159	206	—
	9/27/2005	13:15–13:45	—	140	—	—	1.4	—	—	1.14	—	—	211	—
	9/27/2005	16:00–16:30	—	135	—	—	2.1	—	—	1.09	—	—	208	—
	10/11/2005	10:45–11:30	50	130	—	1.4	2.0	—	0.41	1.05	—	149	206	—
	10/11/2005	14:15–15:00	80	135	—	1.0	2.4	—	0.65	1.09	—	175	208	—
Fire	9/30/2005	12:15–13:15		120	260		17.0	2.0		0.97	2.11	—	200	259

(Continued on next page)

TABLE 3
Summary of APM measurements conducted in the Los Angeles Basin in September/October 2004 *(Continued)*

			APM Voltage, V			Number Concentration, cm^{-3}			Effective Density, g cm^{-3}			Aerodynamic diameter, nm		
Location	Date	Time	V_1	V_2	V_3	N_1	N_2	N_3	ρ_{e1}	ρ_{e2}	ρ_{e3}	d_{ae1}	d_{ae2}	d_{ae3}
$d_{me} = 322$ nm														
710	9/20/2005	11:15–12:00	150	350	—	0.6	1.1	—	0.21	0.49	—	191	253	—
	9/20/2005	15:15–16:00	110	440	—	1.1	0.8	—	0.15	0.61	—	172	273	—
	9/21/2005	10:15–11:00	100	500	—	1.2	1.4	—	0.14	0.69	—	167	285	—
	9/21/2005	12:40–13:15	140	540	—	1.0	0.6	—	0.19	0.75	—	186	292	—
110	9/26/2005	14:30–15:30	200	570	—	0.2	0.4	—	0.28	0.79	—	210	298	—
	9/26/2005	17:45–18:15	150	—	—	0.2	—	—	0.21	—	—	191	—	—
	9/28/2005	12:30–13:00	200	—	—	0.2	—	—	0.28	—	—	210	—	—
USC	9/12/2005	12:00–13:00	—	530	—	—	0.7	—	—	0.74	—	—	291	—
	9/13/2005	11:00–12:00	—	530	—	—	0.3	—	—	0.74	—	—	291	—
	9/14/2005	12:00–13:00	—	550	—	—	0.9	—	—	0.76	—	—	294	—
	9/14/2005	14:30–15:15	—	510	—	—	0.7	—	—	0.71	—	—	287	—
$d_{me} = 414$ nm														
710	9/20/2005	12:00–13:00	200	700	—	0.9	0.5	—	0.12	0.42	—	204	310	—
	9/20/2005	16:00–16:45	170	900	1000	0.7	0.2	0.3	0.10	0.54	0.60	194	338	350
	9/21/2005	8:00–9:00	200	—	1000	1.8	—	0.7	0.12	—	0.60	204	—	350
	9/21/2005	11:00–11:45	—	—	1100	—	—	0.3	—	—	0.66	—	—	361
USC	9/14/2005	13:45–14:30	—	—	1100	—	—	0.2	—	—	0.66	—	—	361

diesel vehicles, which commonly emit two distinct modes of particles. One mode consists of carbonaceous solid agglomerate particles, occurring between 100–200 nm in mobility diameter, while the more volatile particles exist in the sub-50 nm mode, as discussed earlier (Harris and Maricq 2001; Sakurai et al. 2003; Kuhn et al. 2005a,b). The particles at I-710 appear to be externally mixed with the majority existing as organic droplets and a smaller population of low-density agglomerates. Fractal agglomerate particles of 118 nm mobility diameter were found only on one day and in much lower concentrations at CA-110 because only gasoline vehicle emissions impact the site, which in general tend to emit lower elemental carbon than heavy duty diesel (Schauer et al. 2002). Furthermore, the number distribution rapidly drops off after 50 nm at CA-110, which means that 118 nm particles sampled at this site may likely be more closely associated with the urban background (Kuhn et al. 2005a). Therefore, measured densities between 0.98 and 1.41 g cm^{-3} are probably indicative of complex particles, composed of ammonium nitrate, metals, organic compounds and water (Kuhn et al. 2005b). The majority of 118 nm particles in the coastal site also exhibited an effective density close to 1.26 g cm^{-3}, which is likely due to hydrated sulfate droplets. As argued by Kleeman et al. (1999), the similarity in sulfate concentrations throughout the Los Angeles basin confirms that the majority of the sub-micrometer sulfate aerosol in that area in recent years is advected into the urban area from over the Pacific Ocean, with a minority of the sulfate aerosol formed by atmospheric reactions within the air basin itself. This situation is due to the strict controls on SO_2 emissions that have been adopted in the South Coast Air Basin.

The effective density measured for 118 nm particles at USC is similar to that at I-710 although the lower effective density agglomerates are missing. The site is impacted by mostly light duty and some heavy duty vehicle emissions (although to a much lesser extent than the I-710), and is located sufficiently far downwind from the freeway for nuclei mode particles to grow to that range, as demonstrated by the experimental measurements of Zhu et al. (2002) and the modeling work of Zhang et al. (2005). Supersaturated organic vapors condensing onto the surface of these particles result in densities around 1.0 g cm^{-3}.

An interesting observation is that the density of 118 nm particles was slightly higher than that of 50 nm particles at Riverside. This may be because 118 nm particles are likely an internal mixture of heavier components, such as ammonium nitrate and organic compounds, which form during advection and long range transport of air parcels from Los Angeles to the receptor site of Riverside, situated about 100 km downwind.

Due to time and other experimental field constraints, field measurements of 146 nm particles were only conducted at a few of the sampling locations. At USC, 146 nm particles had a higher effective density ($\rho_e = 1.43$ g cm^{-3}) than 118 nm particles ($\rho_e = 1.05$ g cm^{-3}), which may be due to the additional condensation of higher density species such as ammonium nitrate on to primary particles. It should be noted that in this as

well as other locations of our study, the influence of the nearby freeways decreases with increasing particle size, suggesting that a significant fraction of these larger particles are representative of the urban background aerosol. I-710 particles with 146 nm diameter also exhibited a bimodal distribution, with two significant differences from 118 nm. The higher density mode occurs at $\rho_e = 1.43$ g cm^{-3}, compared to $\rho_e = 1.05$ g cm^{-3} for 118 nm particles. This difference may be explained by a higher contribution of urban background (than freeway) to this particle size or higher association of particle-bound metals and other high-density compounds from the freeway with this particle size. The second difference is that the low-density peak of 146 nm particles ($\rho_e = 0.68$ g cm^{-3}) had a higher number concentration than the high-density peak, which is indicative of a higher percentage of carbonaceous soot agglomerates, directly emitted by diesel vehicles on the freeway, at that mobility diameter. Similar to 118 nm particles, the majority of 146 nm particles at Riverside are part of an aged aerosol transported from Los Angeles, resulting in an effective density of $\rho_e = 1.38 \pm 0.06$ g cm^{-3}. Low densities were measured in the morning and will be discussed in the subsequent section.

Similar to other sizes, 202 nm particles at USC are mostly contained in one large mode with $\rho_e = 1.09 \pm 0.08$ g cm^{-3}, indicative of an internally mixed aerosol of mostly organic chemical composition. The coastal aerosol has a high content of 202 nm particles with effective densities near 1.0 g cm^{-3}, which is probably due to the large amount of water associated with hygroscopic (mostly sulfate) aerosols in that site. The majority of 202 nm particles at I-710 fit into a bimodal distribution with effective densities of both modes having values less than unity. The lighter fraction ($\rho_e = 0.41 \pm 0$ g cm^{-3}) dominated the heavier one ($\rho_e = 0.93 \pm 0.12$ g cm^{-3}), which could include low-density agglomerates that have been coated with organic vapors, resulting in an increase in effective density. Density in Riverside is still well above unity for a majority of 202 nm particles ($\rho_e = 1.09 \pm 0.03$ g cm^{-3}), but there is a clear decrease when compared to smaller particle sizes. Although particles within the accumulation mode in Riverside are likely to be internally mixed with little dependence of chemical composition on particle diameter, there may be void space or particle bound water associated with the larger particles that reduces the effective density. Similar to 146 nm particles, significant concentrations of low-density particles were measured in the morning.

Unlike other particle sizes, effective densities greater than 2.0 g cm^{-3} were measured for 118 nm and 202 nm particles. The higher effective density particles may reflect complex urban background mixtures of ammonium sulfate, ammonium nitrate, and metals observed in previous field studies in the basin (Hughes et al. 2000). For the marine background aerosols, the larger peak is 0.97–1.26 g cm^{-3}, which is consistent with the density of a hygroscopic aerosol at high relative humidity conditions. The much smaller peak at around 2 g cm^{-3}, based solely on density values, would indicate that sea salt spray generated by breaking waves is most likely the source. Sea salt spray is composed of sodium chloride particles, which have a bulk density of 2.16 g cm^{-3}. Although previous studies showed that ocean spray generates super-micrometer particles (Kleeman et al. 1999), it is conceivable that the measured particles represent a "tail" in the size distribution of coarser sodium chloride PM.

McMurry et al. (2002) also reported particle densities close to 2.0 g cm^{-3} for 309 nm particles on multiple occasions. While no conclusions were drawn about the chemical composition of these particles, the authors of that study did rule out multiple charging as the source of this signal. It is unlikely that multiply charged particles are contributing to this secondary mode here because number concentration decreases rapidly with increasing particle diameter, and the number of multiply charged particles is a very minute fraction of total concentration.

During our sampling period, a brush fire occurred in Southern California, which provided a unique opportunity to determine effective densities of fire emission particles. Because of the relatively unstable nature of this event due to the changes in both fire and wind direction, only two sizes, i.e., 118 nm and 202 nm, could be measured. The particle density is roughly around unity for 202 nm and 1.4 g cm^{-3} for 118 nm particles. A previous study in Southern California reported size distributions with a mode diameter of 100–200 nm for particles emitted by forest fires (Phuleria et al. 2005b). The chemical composition of $PM_{2.5}$ emitted by wood burning and prescribed burns has been shown to be dominated by organic carbon (Kleeman et al. 1999; Robinson et al. 2004). The average of the bulk densities of the various organic species could result in the reported effective densities. Another study found wood combustion particles, although composed of small primary particles, to be compact in shape instead of fractal (Colbeck et al. 1997). This may explain fire-emitted particle effective densities greater than or equal to unity.

Because 322 nm particles are less abundant in the atmosphere, concentrations at all locations approached the noise level of the CPC. No data could be reported for Riverside and the coast. Regardless of the site, the effective density of 322 nm particles was almost invariably smaller than unity. The probability that particles are fractal agglomerates, which have associated void spaces, would likely increase with particle diameter because these particles are often altered by atmospheric transformations and have the potential to scavenge smaller particles. The two freeway locations both exhibit two distinct effective densities, at 0.14–0.28 g cm^{-3} and 0.49–0.79 g cm^{-3}. The lower end of the range of each is found at I-710, which is likely influenced by the increased presence of carbon-rich fractal agglomerates from diesel emissions at this site. The existence of an effective density mode around 0.6–0.8 g cm^{-3} at each site may signify that a fraction of 322 nm particles is regional in nature.

Similar detection limit problems occurred for 414 nm particles that were found for 322 nm particles. The very low concentrations, which were often less than 1 particle per cm^3, increased sampling uncertainty so that conclusive data could only be recorded at USC and I-710. As with 322 nm, all 414 nm

particles have effective densities below unity, and the reasons for this are likely similar to those presented for 322 nm particles above. A very low-density (ρ_e ~0.1) population of particles was measured at I-710.

Diurnal Variability of Particle Density at Riverside

The relative consistency of the vehicle emissions that are the dominant aerosol source at the freeway sites (I-710 and CA-110) made it difficult to draw any meaningful conclusions concerning diurnal variation of effective density in these locations. Limited data at the coast also prevented analysis of diurnal variability. Riverside was selected as the site at which to conduct multiple measurements in order to investigate diurnal variability of particle effective density because of its consistent daily meteorological variation (e.g., temperature, relativity, and wind velocity vary similarly from day to day). The daily fluctuation in wind velocity at Riverside generally favors the impact of local sources in the mornings, whereas afternoons are dominated by photochemically produced aerosols as well as regional aerosols advected to that site from urban upwind locations (Kim et al. 2002; Fine et al. 2004).

As reported in an earlier section, photochemical byproducts were thought to attribute to the effective density of 50 nm particles at Riverside ($\rho_e \sim 1.4$ g cm^{-3}). Figure 5 further illustrates the possible effect of photochemical formation on the effective density for 50 nm particles. Hourly data have been plotted from 11 October 2005, during which the temperature peaked at 28°C between 13:00 and 15:00. The effective particle density during this time period was 1.35–1.4 g cm^{-3}. As the sun angle rapidly decreased and temperature declined to 23°C after 16:00, the particle density dropped to a value of 1.2 g cm^{-3}.

Particles between 118–202 nm have either a shoulder or second mode that occurs only in the morning. Figure 6 displays the diurnal variation in effective density for 146 nm particles. A significant number of morning particles exhibit densities less than unity, which is probably an effect of local morning traffic emissions that can affect the site due to stagnant conditions. In addition to visible morning traffic effects, effective density at Riverside varied slightly throughout the afternoon. The possible effect of photochemistry on 50 nm particles has been previously discussed, but particles between 118–202 nm also increase in effective density as the day progresses from morning to afternoon. It is likely that the stronger advection in the afternoon transports particles with higher proportions of SOA and ammonium salts, while particles lose water as temperatures rise.

Dependence of Effective Density on Particle Diameter

From the results of the five particle sizes studied, it is evident that effective density decreases with increasing particle mobility diameter. This phenomenon appears to occur regardless of starting density and location. Figures 7–9 show the relationship between particle effective density and mobility diameter at I-710, CA-110 and USC, respectively. At I-710 all particle sizes other than 50 nm have two effective densities associated with each. These densities appear to align themselves into two groups: a high effective density line, and a low effective density line. Both lines decrease with the same slope, which suggests particle mobility diameter is an important indicator of effective density. Although not as many data points are available, a similar trend is observed at CA-110, and effective density decreases with increasing particle diameter at USC for $d_p > 200$ nm. In accordance with Equation (2), effective densities of larger agglomerates were determined to be lower than those of smaller agglomerates, which is likely due to an increase in void space with agglomerate diameter. Fuchs (1964) opined that effective density might vary 0.1 to 0.7 times the primary particle density, while Pontikakis (2001) assumed effective densities as low as 0.05 g cm^{-3} for modeling of diesel particle retention filters. The

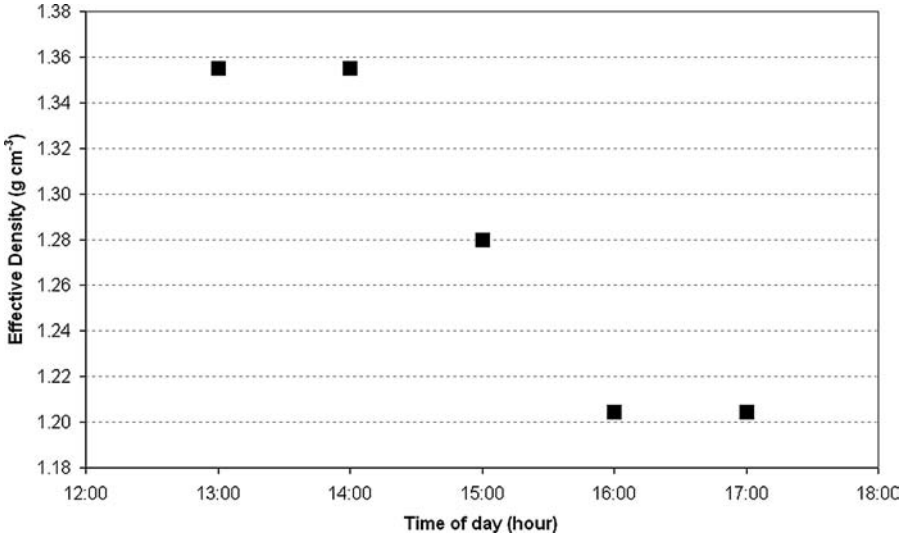

FIG. 5. Diurnal variation of effective density for 50 nm atmospheric particles in Riverside, CA.

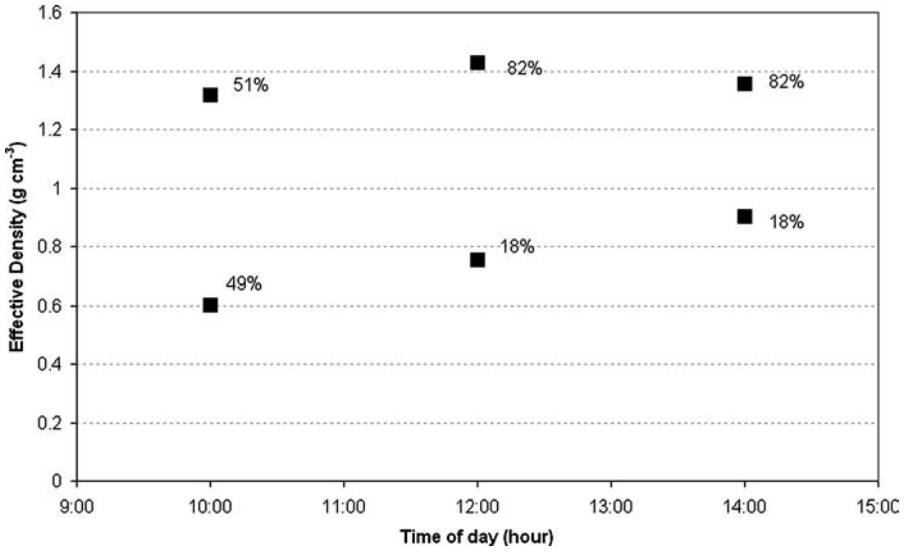

FIG. 6. Diurnal variation of effective density for 146 nm atmospheric particles in Riverside, CA.

results of this study corroborate these arguments and imply the possible existence of density as low as 0.05 g cm^{-3}.

Table 4 summarizes the effective densities and fractal dimensions reported for all sites and particle sizes sampled. Effective densities are averaged by particle size and site without consideration of diurnal variation by calculating the centroid APM voltage from each scan. Laboratory experiments with spherical particles show particles of different masses penetrate the APM at a particular voltage, which broadens the distribution, but the centroid voltage and peak voltage are nearly equal due to the symmetry of this distribution. The shoulders seen in atmospheric voltage scans are due to particles with different shapes and/or densities. Thus, taking the centroid voltage of a scan with multiple voltage peaks will be minimally affected by APM separation efficiency while weighting the average effective density based on number concentration measured at each voltage. As previously mentioned, size-averaged effective density decreases with increasing particle mobility diameter for all effective densities. This effect is most prominent for I-710, where larger particles (414 nm) demonstrated average ρ_e as low as 0.31 g cm^{-3}. Ahlvik et al. (1998) and Park et al. (2003) also reported similar low effective densities for diluted diesel exhaust aerosols with a DMA followed by an ELPI and APM, respectively. The effective density of the marine aerosol did not show much variation, with

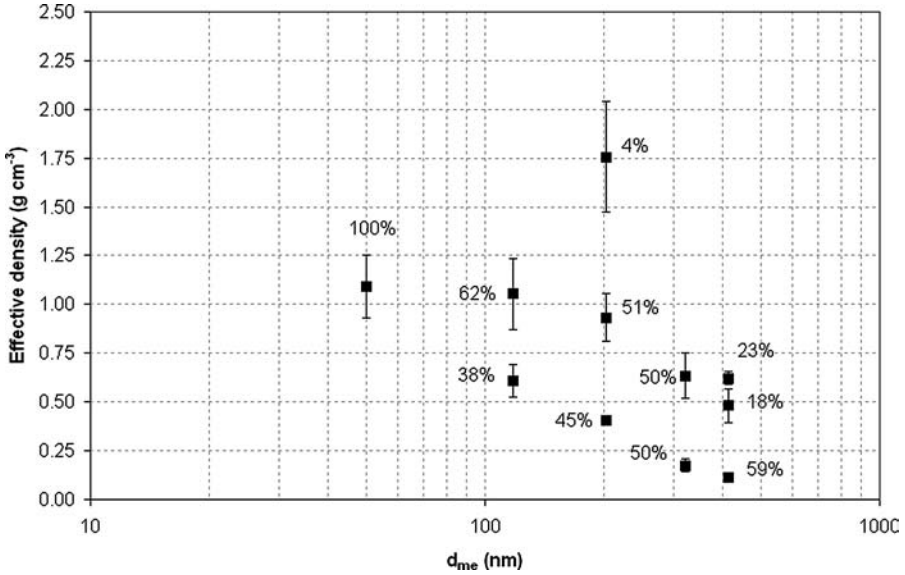

FIG. 7. Effective density variation with respect to particle mobility diameter at I-710. Data labels indicate percentage of number concentration measured for each particle size with respective effective density.

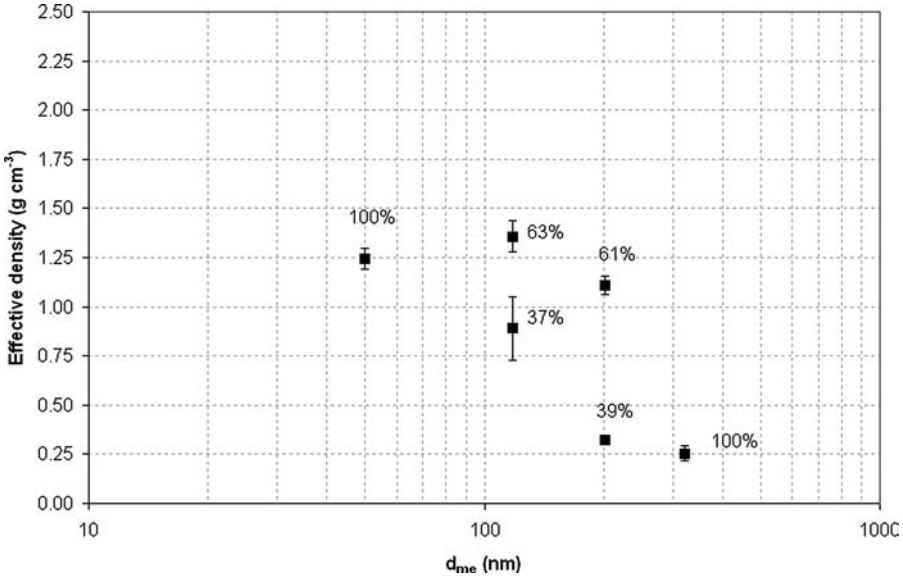

FIG. 8. Effective density variation with respect to particle mobility diameter at CA-110. Data labels indicate percentage of number concentration measured for each particle size with respective effective density.

$\rho_e \sim 1.0$ g cm^{-3} for all particle sizes. Salt particles may absorb a significant amount of moisture and dissolve into droplets, which mask any irregularities in shape. Riverside is characterized by high-density ($\rho_e > 1$) particles between 50 and 202 nm in diameter, mostly the result of photochemical processes and advection of the Los Angeles urban plume upwind of that site. Irrespective of site, 322 nm and 414 nm particles have densities less than unity. Although vehicle sources are known to emit carbonaceous agglomerates, particles of these two sizes may also be agglomerates of other primary atmospheric particles formed during coagulation and atmospheric chemical reactions.

Estimates of Aerosol Fractal Dimension

The fractal dimension for each location was calculated from Equation (2) by plotting the logarithm of mobility diameter versus the logarithm of average effective density values in Table 4. Fractal dimension can increase with the presence of water, so it is not surprising that the highest fractal dimension was found at the coast ($D_f = 2.92 \pm 0.15$). The lack of combustion emissions

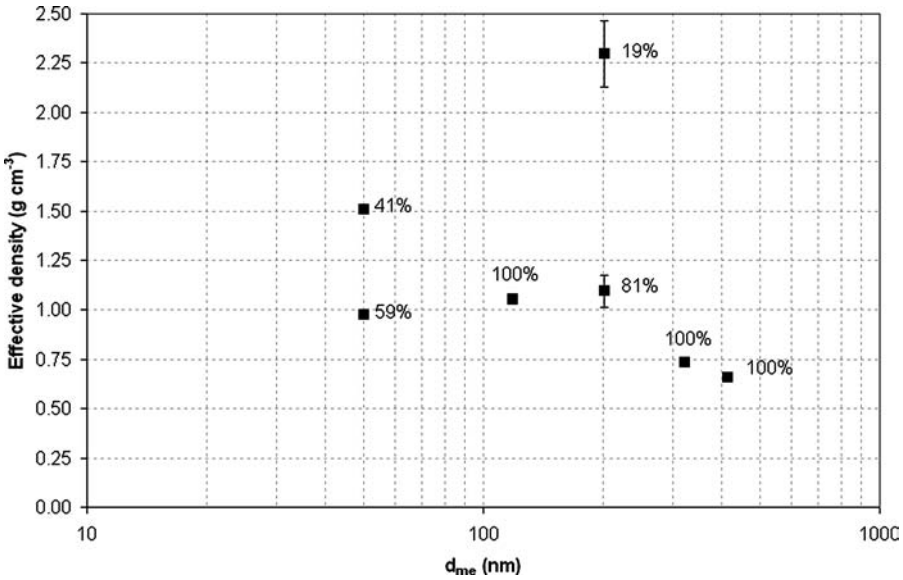

FIG. 9. Effective density variation with respect to particle mobility diameter at USC. Data labels indicate percentage of number concentration measured for each particle size with respective effective density.

TABLE 4
Summary of average effective densities of different field locations and their fractal dimensions

Mobility diameter (d_m, nm)	Average effective density (ρ_e), g cm^{-3}				
	USC	710-freeway	110-freeway	Riverside	Coast
50	1.14 ± 0.1	1.13 ± 0.10	1.45 ± 0.12	1.40 ± 0.10	1.19 ± 0.10
118	1.12 ± 0.14	1.00 ± 0.12	1.17 ± 0.02	1.40 ± 0.06	1.14 ± 0.23
146	1.21 ± 0.08	0.94 ± 0.16	NA	1.29 ± 0.06	0.99 ± 0.10
202	1.14 ± 0.24	0.78 ± 0.26	0.99 ± 0.09	1.06 ± 0.09	1.06 ± 0.20
322	0.86 ± 0.11	0.49 ± 0.07	0.59 ± 0.27	NA	NA
414	0.73 ± 0.10	0.31 ± 0.02	0.58 ± 0.06	NA	NA
Fractal dimension	2.79 ± 0.15	2.41 ± 0.22	2.54 ± 0.28	2.83 ± 0.06	2.92 ± 0.15

at this site also validates this result. Conversely, the I-710 fractal dimension was the lowest of all sites ($D_f = 2.41 \pm 0.22$), presumably due to the much higher contribution of diesel trucks at that location. Previous dynamometer studies have reported a fractal dimension of 2.3 ± 0.1 for vehicle exhaust with DMA-ELPI and DMA-APM systems, which is in good agreement with the current I-710 results (Maricq et al. 2004; Van Gujik et al. 2004; Park et al. 2003). Diesel freeway aerosols may have higher fractal dimensions than pure diesel exhaust due to changes in particles between the tailpipe and the sample inlet as organic vapors condense on soot particles when exhaust gases mix with cold air (Kittelson 1998).

CA-110 freeway aerosols had a fractal dimension slightly higher than I-710 ($D_f = 2.54 \pm 0.28$), indicating that gasoline vehicles generate chain agglomerates, especially in the higher range of particles (>200 nm). Particles at USC did not have a particularly low fractal dimension ($D_f = 2.79 \pm 0.15$), although these particles may contain significant amounts of elemental carbon (Sardar et al. 2005). The USC location is much farther from vehicle sources than the two freeway sites. Because fractal agglomerates have a very high surface area, it is conceivable that they are altered by vapor condensation, adsorption and/or scavenging between the time of emission and the time of sampling at USC. This will lead to morphological changes of the original aggregate particle to become more compact. Finally, the fractal dimension in Riverside was calculated as 2.83 ± 0.06. Because Riverside is significantly downwind of the freshly emitted particles from Los Angeles, these particles undergo many changes due to temperature, relative humidity, and chemical reactions before reaching Riverside. All of these will have an effect on particle morphology. It is unknown, however, if fractal agglomerates retain their structure within a droplet or if they become more compact due to alterations in the primary particle arrangement.

SUMMARY AND CONCLUSIONS

This study employed a previously developed tandem of the APM and SMPS to determine in-situ effective density of atmospheric particles over a mobility size range of 50–414 nm. Field-testing of ambient particles revealed effective density of unity or more for 50 nm particles, indicative of their spherical nature. The lower density of marine aerosols may be due to the presence of a significant amount of organics. Riverside aerosols, with an effective density as high as 1.4–1.5 g cm^{-3} for this particle size, are thought to be generated predominantly from photochemical reactions.

A significant number of particles at I-710 may be chain agglomerates, which is demonstrated by the bimodal density distribution measured there. The majority of 118 nm and 146 nm particles, however, are internally mixed, originating from background urban sources. Morning traffic can produce a bimodal density distribution for these particles similar to that of I-710, as shown by the diurnal variation at Riverside. CA-110 freeway exhibited low-density 202 nm particles, generated from gasoline-powered vehicles. The urban and marine background sources have a higher density fraction at 202 nm mobility size, which most likely is comprised of ammonium sulfate, ammonium nitrate, and metals.

Low concentrations of 322 nm and 414 nm particles increased sampling uncertainty at some locations. The effective density for these particles is very low, ranging from 0.1 to 0.7 g cm^{-3}. Densities this low are explained by the high probability that these particles have void space associated with them. It is evident from the results that with the increase in particle size, effective density decreased irrespective of location. Thus, it can be concluded that particle morphology varied from nearly solid spheres in the small sizes to agglomerate chains at higher sizes.

Although not the focus of this study, diurnal density variation was revealed at Riverside, CA. Low effective density particles are present in the morning, due to the influence of local traffic, but these particles disappear in the afternoon. In addition, the effective density of both smaller and larger particles increases in the afternoon, presumably due to increased photochemistry and higher proportion of secondary organic aerosols. A more comprehensive examination of diurnal effects at various sites merits future consideration.

Calculated fractal dimensions yielded predictable results, with $D_f = 2.41$ for Interstate 710, a freeway with a high

heavy-duty diesel vehicle traffic. Similarly, a low average particle fractal dimension (2.54) was found at the gasoline vehicle dominated freeway (CA-110), which is also affected by the presence of chain agglomerates. The fractal dimensions at USC, Riverside and the coast were 2.79, 2.87, and 2.92, respectively, indicating that overall the average shape of particles in these locations approaches that of a sphere. As one would expect, fractal dimension increases with distance from traffic emissions across these sites. The higher fractal dimension at USC compared to the freeway sites demonstrates that fractals diminish quickly with distance away from freeway, which may be due to vapor condensation-adsorption on particles. Fractal dimensions approach 3.0 at Riverside and the coast due to the much lower impact of emissions from combustion processes at these sites.

REFERENCES

Ahlvik, P., Ntziachristos, L., Keskinen, J., and Virtanen, A. (1998). Real Time Measurements of Diesel Particle Size Distribution with an Electrical Low Pressure Impactor, *SAE Tech. Pap.* No. 980410.

Bahreini R., Keywood, M. D., Ng, N. L., Varutbangkul, V., Gao, S., Flagan, R. C., Seinfeld, J. H., Worsnop, D. R., and Jimenez, J. L. (2005). Measurements of Secondary Organic Aerosol from Oxidation of Cycloalkenes, Terpenes, and m-Xylene using an Aerodyne Aerosol Mass Spectrometer, *Environ. Sci. Technol*. 39:5674–5688.

Biswas, S., Fine, P. M., Geller, M. D., Hering, S. V, and Sioutas, C. (2004). Performance Evaluation of a Recently Developed Water-Based Condensation Particle Counter, *Aerosol Sci. Technol.* 39:419–427.

Blando, J. D., and Turpin, B. J. (2000). Secondary Organic Aerosol Formation in Cloud and Fog Droplets: A Literature Evaluation of Plausibility, *Atmos. Environ.* 34:1623–1632.

Burtscher, H. (2005). Physical Characterization of Particulate Emissions from Diesel, *J. Aerosol Sci.* 36:896–932.

Colbeck, I., Atkinson, B., and Johar, Y. (1997). The Morphology and Optical Properties of Soot Produced by Different Fuels, *J. Aerosol Sci.* 28(5): 715–723.

Dockery, D. W., and Pope, C. A., III (1994). Acute Respiratory Effects of Particulate Air Pollution, *Ann. Rev. Public Health* 15:107–132.

Ehara, K., Hagwood, C., and Coakley, K. J. (1996). Novel Method to Classify Aerosol Particles According to their Mass-to-Charge Ratio Aerosol Particle Mass Analyzer, *J. Aerosol Sci.* 27:217–234.

Fine, P. M., Shen, S., and Sioutas, C. (2004). Inferring the Sources of Fine and Ultrafine Particulate Matter at Downwind Receptor Sites in the Los Angeles Basin using Multiple Continuous Measurements, *Aerosol Sci. Technol.* 38:182–195.

Fuchs, N. A. (1964), *The Mechanics of Aerosols*, Pergamon Press, Oxford.

Geller, M. D., Kim, S. Misra, C., Sioutas, C., Olson, B. A., and Marple, V. A. (2002). Methodology for Measuring Size-Dependent Chemical Composition of Ultrafine Particles, *Aerosol Sci. Technol.* 36:748–763.

Hänel, G., and Thudium, J. (1977) Mean Bulk Densities of Samples of Dry Atmospheric Aerosol Particles-Summary of Measured Data, *Pure Appl. Geophys.* 115(4): 799–803.

Harris, S. J., and Maricq, M. M. (2001). Signature Size Distributions for Diesel and Gasoline Engine Exhaust Particulate Matter, *J. Aerosol Sci.* 32: 749–764.

Hughes, L. S., Allen, J. O., Kleeman, M. J., Johnson, R. J., Cass, G. R., Gross, D. S., Gard, E. E., Galli, M. E., Morrical, B. D., Fergenson, D. P., Dienes, T., Noble, C. A., Silva, P. J., and Prather, K. A. (1999). Size and Composition Distribution of Atmospheric Particles in Southern California, *Environ. Sci. Technol.* 33(20): 3506–3515.

Hughes, L. S., Allen, J. O., Bhave, P., Kleeman, M. J., Cass, G. R., Liu, D. Y., Fergenson, D. P, Morrical, B. D., and Prather, K. A. (2000). Evolution of Atmospheric Particles along Trajectories Crossing the Los Angeles Basin, *Environ. Sci. Technol.* 34:3058–3068.

Jaffe, D., Tamuraa, S., and Harrisb, J. (2005). Seasonal Cycle and Composition of Background Fine Particles along the West Coast of the US, *Atmos. Environ.* 39:297–306.

Jang, M. S., Czoschke, N. M., Lee, S., and Kamens, R. M. (2002). Heterogeneous Atmospheric Aerosol Production by Acid-Catalyzed Particle-Phase Reactions, *Science* 298: 814–817.

Keskinen, J., Virtanen, A. Ahlvik, P., and Ntziachristos, L. (1998). Estimation of Effective Density of Diesel Particles, *J. Aerosol Sci.* 29:S1007–S1008.

Khlystov, A., Stanier, C., and Pandis, S. N. (2004). An Algorithm for Combining Electrical Mobility and Aerodynamic Size Distributions Data when Measuring Ambient Aerosol, *Aerosol Sci. Technol.* 38(S1):229–238.

Kim, S., Shi, S., Zhu, Y., Hinds, W. C., and Sioutas, C. (2002). Size Distribution, Diurnal and Seasonal Trends of Ultrafine Particles in Source and Receptor Sites of the Los Angeles Basin, *J. Air Waste Manage. Assoc.* 52:174–185.

Kittelson, D. B. (1998). Engines and Nanoparticles: A Review, *J. Aerosol Sci.* 29: 575–588.

Kleeman, M. J., Hughes, L. S., Allen, J. O., and Cass, G. R. (1999). Source Contributions of the Size and Composition Distribution of Atmospheric Particles: Southern California in September 1996, *Environ. Sci. Technol.* 33:4331–4341.

Kuhlbusch, T. A. J., John, A. C., and Fissan, H. (2001). Diurnal Variations of Aerosol Characteristics at a Rural Measuring Site Close to the Ruhr-Area, Germany, *Atmos. Environ.* 35:S13–S21.

Kuhn, T., Biswas, S., Fine, P. M., Geller, M. D., and Sioutas C. (2005a). Physical and Chemical Characteristics and Volatility of PM in the Proximity of a Light-Duty Vehicle Freeway, *Aerosol. Sci. Technol.* 39:347–357.

Kuhn, T., Biswas, S., and Sioutas, C. (2005b). Diurnal and Seasonal Characteristics of Particle Volatility and Chemical Composition Near a Light-Duty Vehicle Freeway, *Atmos. Environ.* 39:7154–7166.

Kutz, S., and Schmidt-Ott, A. (1990). Use of a Low-Pressure Impactor for Fractal Analysis of Sub-Micron Particles, *J. Aerosol Sci.* 21:S47–S50.

Li N., Sioutas C., Cho A., Schmitz D., Misra C., Sempf J., Wang M. Y., Oberley T., Froines J., and Nel A. (2003). Ultrafine Particulate Pollutants Induce Oxidative Stress and Mitochondrial Damage, *Environ. Health Persp.* 111: 455–460.

Maricq, M. M., Podsiadlik, D. H., and Chase, R. E. (2000). Size Distributions of Motor Vehicle Exhaust PM: A Comparison between ELPI and SMPS Measurements, *Aerosol Sci. Technol*. 33:239–260.

Maricq, M. M., and Xu, N. (2004). The Effective Density and Fractal Dimension of Soot Particles from Premixed Flames and Motor Vehicle Exhaust, *J. Aerosol Sci.* 35:1251–1274.

McMurry, P. H., Wang, X., Park, K., and Ehara, K. (2002). The Relationship Between Mass and Mobility for Atmospheric Particles: A New Technique for Measuring Particle Density, *Aerosol Sci. Technol.* 36:227–238.

Morawska, L., Johnson, G., Ristovski, Z. D., and Agranovski, V. (1999). Relation Between Particle Mass and Number for Sub Micrometer Airborne Particles, *Atmos. Environ.* 33:1983–1990.

Oberdörster, G. (1996). Significance of Particle Parameters in the Evaluation of Exposure-Dose-Response Relationships of Inhaled Particles, *Part. Sci. Technol.* 14(2):135–151.

Park, K., Feng, C., Kittelson, D. B., and McMurry, P. H. (2003). Relationship between Particle Mass and Mobility, and between Aerodynamic and Mobility Size Distributions for Diesel Exhaust Particles, *Environ. Sci. Technol.* 37:577–583.

Park, K., Kittelson, D. B., and McMurry, P. H. (2004). Structural Properties of Diesel Exhaust Particles Measured by Transmission Electron Microscopy (TEM): Relationships to Particle Mass and Mobility, *Aerosol Sci. Technol.* 38:881–889.

Peters, A., Wichmann, H. E., Tuch, T., Heinrich, J., and Heyder, J. (1997). Respiratory Effects are Associated with the Number of Ultrafine Particles, *Am. J. Respir Crit. Care Med.* 155:1376–1383.

Phuleria, H., Geller, M. D., Fine, P. M., and Sioutas, C. Size-Resolved Emissions of Organic Tracers from Light and Heavy-Duty Vehicles Measured in a

California Roadway Tunnel, Submitted for publication to *Environ. Sci. Technol*., in press, June 2006.

Phuleria, H., Fine, P. M., Zhu, Y., and Sioutas, C. (2005b). Characterization of Particulate Matter and Co-pollutants during the Fall 2003 Southern California fires, *J. Geophys. Res.* 110(D7):Art. No. D07S20.

Pitz, M., Cyrys, J., Karg, E., Wiedensohler, A., Wichmann, H. E., and Heinrich, J. (2003). Variability of Apparent Particle Density of an Urban Aerosol, *Environ. Sci. Technol.* 37:4336–4342.

Pontikakis, G. N., Koltsakis, G. C., and Stamatelos, A. M. (2001). Dynamic Filtration Modeling in Foam Filters for Diesel Exhaust, *Chem. Eng. Commun.* 188:21–46.

Robinson, M. S., Chavez, J., Velazquez, S., and Jayanty, R. K. M. (2004). Chemical Speciation of PM2.5 Fires of the Coconino National Collected during Prescribed Forest near Flagstaff, Arizona, *J. Air Waste Manage. Assoc.* 54(9):1112–1123.

Sakurai, H., Tobias, H. J., Park, K., Zarling, D., Docherty, S., Kittelson, D. B., McMurry, P. H., and Ziemann, P. J. (2003). On-line Measurements of Diesel Nanoparticle Composition and Volatility, *Atmos. Environ.* 37:1199–1210.

Sardar, S. B., Fine, P. M, Mayo, P. R., and Sioutas, C. (2005). Size-Fractionated Measurements of Ambient Ultrafine Particle Chemical Composition in Los Angeles using the Nano-MOUDI, *Environ. Sci. Technol.* 39:932–944.

Schauer, J. J., Kleeman, M. J., Cass, G. R., and Simoneit, B. R. T. (2002). Measurement of Emissions from Air Pollution Sources. 5. C-1-C-32 Organic Compounds from Gasoline-Powered Motor Vehicles, *Environ. Sci. Technol.* 36(6):1169–1180.

Schauer, J. J., Kleeman, M. J., Cass, G. R., and Simoneit, B. R. T. (1999). Measurement of Emissions from Air Pollution Sources. 2. C1 through C_{30} Organic Compounds from Medium Duty Diesel Trucks, *Environ. Sci. Technol.* 33:1578–1587.

Sharma, M., Agarwal, A. K., and Bharathi K. V. L. (2005). Characterization of Exhaust Particulates from Diesel Engine, *Atmos. Environ.* 39:3023–3028.

Turpin, B. J., and Lim, H.-J. (2001). Species Contributions to PM2.5 Mass Concentrations: Revisiting Common Assumptions for Estimating Organic Mass, *Aerosol Sci. Technol.* 35:602–610.

Van Gulijk, C., Marijnissen, J. C. M., Makkee, M., Moulijn, J. A., and Schmidt-Ott, A. (2004). Measuring Diesel Soot with a Scanning Mobility Particle Sizer and an Electrical Low-Pressure Impactor: Performance Assessment with a Model for Fractal-like Agglomerates, *J. Aerosol Sci.* 35:633–655.

Van Gulijk, C., Schouten, H., Marijnissen, J. C. M., Makkee, M., and Moulijn, J. A. (2001). Restriction for the ELPI in Diesel Particulate Measurements, *J. Aerosol Sci*. 32:1117–1130.

Virtanen, A., Ristimaki, J., and Keskinen, J. (2004). Method for Measuring Effective Density and Fractal Dimension of Aerosol Agglomerates, *Aerosol Sci. Technol.* 38:437–446.

Wentzel, M., Gorzawski, H., Naumann, K.-H., Saathoff, H., and Weinbruch, S. (2003). Transmission Electron Microscopical and Aerosol Dynamical Characterization of Soot Aerosols, *J. Aerosol Sci.* 34:1347–1370.

Zhang, K. M., Wexler, A. S., Niemeier, D. A., Zhu, Y. F., Hinds, W. C., and Sioutas, C. (2005). Evolution of Particle Number Distribution Near Roadways. Part III: Traffic Analysis and On-road Size Resolved Particulate Emission Factors, *Atmos. Environ.* 39:4155–4166.

Zhu, Y. C., Hinds, W. C., Kim, S., Shen, S., and Sioutas, C. (2002). Study of Ultrafine Particles Near a Major Highway with Heavy-duty Diesel Traffic, *Atmos. Environ.* 36:4323–4335.

Zielinska, B., Sagebiel, J., Arnott, W. P., Rogers, C. F., Kelly, K. E., Wagner, D. A. Lighty, J. S., Sarofim, A. F., and Palmer, G. (2004). Phase and Size Distribution of Polycyclic Aromatic Hydrocarbons in Diesel and Gasoline Vehicle Emissions, *Environ. Sci. Technol.* 38:2557–2567.